RESEARCH ARTICLE

Nystagmus in patients with congenital stationary night blindness (CSNB) originates from synchronously firing retinal ganglion cells

Beerend H. J. Winkelman[1,2☯], **Marcus H. C. Howlett**[1☯], **Maj-Britt Hölzel**[1☯], **Coen Joling**[1], **Kathryn H. Fransen**[3,4], **Gobinda Pangeni**[3,4], **Sander Kamermans**[5], **Hiraki Sakuta**[6], **Masaharu Noda**[6], **Huibert J. Simonsz**[1,7], **Maureen A. McCall**[3,4], **Chris I. De Zeeuw**[1,2], **Maarten Kamermans**[1,8]*

1 Netherlands Institute for Neuroscience, Amsterdam, the Netherlands, 2 Department of Neuroscience, Erasmus MC, Rotterdam, the Netherlands, 3 Department of Ophthalmology and Visual Sciences, University of Louisville, Louisville, Kentucky, United States of America, 4 Department of Anatomical Sciences and Neurobiology, University of Louisville, Louisville, Kentucky, United States of America, 5 Polder Animation, Utrecht, the Netherlands, 6 National Institute for Basic Biology, Okazaki, Japan, 7 Department of Ophthalmology, Erasmus MC, Rotterdam, the Netherlands, 8 Department of Biomedical Physics, Academic Medical Center, University of Amsterdam, the Netherlands

☯ These authors contributed equally to this work.
* m.kamermans@nin.knaw.nl

Abstract

Congenital nystagmus, involuntary oscillating small eye movements, is commonly thought to originate from aberrant interactions between brainstem nuclei and foveal cortical pathways. Here, we investigated whether nystagmus associated with congenital stationary night blindness (CSNB) results from primary deficits in the retina. We found that CSNB patients as well as an animal model (*nob* mice), both of which lacked functional nyctalopin protein (NYX, nyx) in ON bipolar cells (BCs) at their synapse with photoreceptors, showed oscillating eye movements at a frequency of 4–7 Hz. *nob* ON direction-selective ganglion cells (DSGCs), which detect global motion and project to the accessory optic system (AOS), oscillated with the same frequency as their eyes. In the dark, individual ganglion cells (GCs) oscillated asynchronously, but their oscillations became synchronized by light stimulation. Likewise, both patient and *nob* mice oscillating eye movements were only present in the light when contrast was present. Retinal pharmacological and genetic manipulations that blocked *nob* GC oscillations also eliminated their oscillating eye movements, and retinal pharmacological manipulations that reduced the oscillation frequency of *nob* GCs also reduced the oscillation frequency of their eye movements. We conclude that, in *nob* mice, synchronized oscillations of retinal GCs, most likely the ON-DCGCs, cause nystagmus with properties similar to those associated with CSNB in humans. These results show that the *nob* mouse is the first animal model for a form of congenital nystagmus, paving the way for development of therapeutic strategies.

Introduction

Congenital nystagmus (i.e., involuntary repetitive uncontrolled eye movements) [1,2] forms a heterogeneous group of eye-movement disorders with eye movements ranging from sinusoidal-like oscillations (pendular nystagmus) to highly asymmetrical repetitive eye movements (jerk nystagmus). Many patients suffering from congenital nystagmus also have a low visual acuity, which limits the quality of life. Congenital nystagmus is commonly thought to originate from aberrant interactions between brainstem nuclei and foveal cortical pathways. However, decades of research has yet to uncover the underlying pathophysiological mechanism(s) of congenital nystagmus or its associated reduced vision.

Our recent clinical research indicated that some types of congenital nystagmus may have a retinal origin [3]. We examined 11 infant boys aged 2 mo through 2 y who presented with a tonic downgaze of both eyes, a chin-up head posture, and a rapid horizontal congenital nystagmus. These infants also had congenital stationary night blindness (CSNB), reduced visual acuity, and mutations in either nyctalopin (*NYX*) or the L-type voltage-gated Ca-channel subunit 1F (*CACNA1F*) genes [3]. These proteins are highly specific to the photoreceptor to ON bipolar cells (BCs) synapse. NYX is located postsynaptically on the ON-BC dendrites [4,5], whereas CACNA1F is expressed presynaptically at the photoreceptor synaptic terminal [6–9]. Mutations in either of these genes abolish ON-BC light responses [8–11].

Here, we studied eye movements of *nob* mice, which lack nyx and are a well-established model for CSNB [7,8]. Strikingly, *nob* mice have a pendular nystagmus with a frequency similar to that found in young CSNB patients. Further analysis of retinal processing and eye movements shows that the oscillating eye movements are caused by a mechanism within the retina that induces synchronized oscillations in retinal ganglion cells (GCs), including the ON direction-selective retinal ganglion cells (DSGCs) that project to the accessory optic system (AOS). Our results show that this form of congenital nystagmus has a retinal origin.

Results

We reanalyzed video material of a group of young children (3 mo–2 y) with a disconjugate small-amplitude horizontal pendular nystagmus in combination with tonic downgaze [3]. These patients had mutations in genes coding for proteins expressed at the synapse between photoreceptors and ON-BCs [3]. The oscillation frequency of their horizontal pendular nystagmus was 6.25 ± 0.63 Hz (*n* = 3) (S1 Fig & S1 Movie). Because one of the patients carried a mutation in the *NYX* gene, we analyzed the eye movements of *nob* mice, which also lack functional NYX protein and are a well-established model of CSNB [7,8]. wt (wild-type) mice (Fig 1A, blue lines) followed a horizontally moving vertical sinusoidal grating (100% contrast, spatial frequency 0.1 cycles/deg, velocity: 10 deg/s) with smooth eye movements and kept their eyes fixated when the stimulus stopped (gray bars). In contrast, the *nob* littermates (red lines) initially followed the same horizontally moving vertical grating with smooth eye movements, but they could not maintain that movement, and they could not fixate their eyes when the grating stopped moving. Regardless of stimulus motion, they had spontaneous, small-amplitude oscillating horizontal eye movements (Fig 1A & 1B). Power spectral density (PSD) plots show that *nob* eye-movement oscillation frequency was approximately 5 Hz, both during the stationary (Fig 1C, solid red lines) and the moving phases (Fig 1C, dashed red lines) of optokinetic stimulation, whereas wt eye movements during both stationary and moving phases had no such peak (Fig 1C, solid and dashed blue lines, respectively). On average, the oscillation frequency of *nob* eye movements to stationary gratings was 5.17 ± 0.18 Hz (*n* = 17) (Fig 1C, solid red line, S2A Fig).
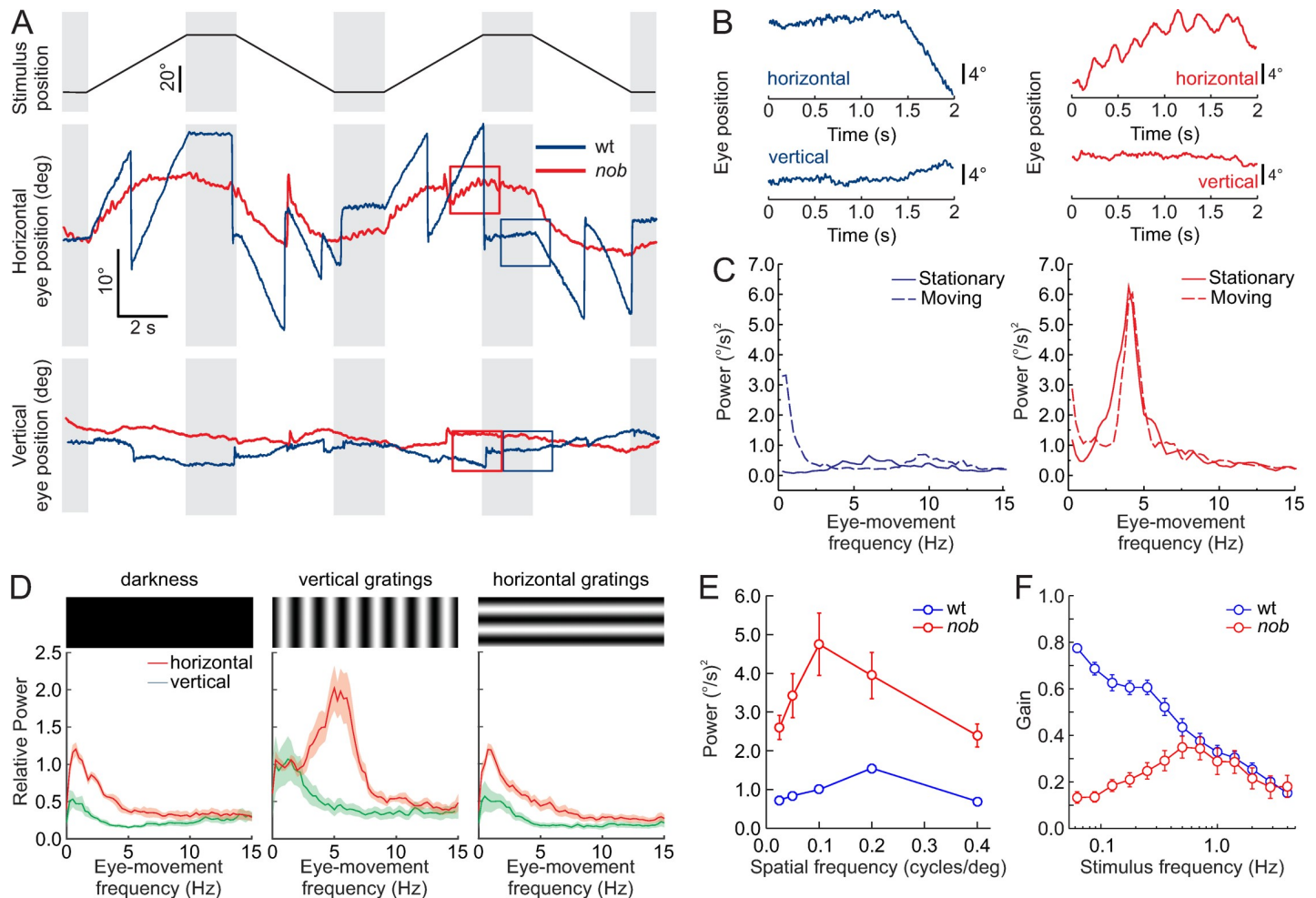
Fig 1. Horizontal eye movements are disturbed in *nob* mice. (A) Schematic diagram of the timing of the stimulus used to evoke eye movements: 0.1 cycle/deg sine wave grating stimulus of 90% contrast moving at 10 deg/s (Top panel). Raw horizontal (middle panel) and vertical (bottom panel) eye movements are compared for wt (blue lines) and *nob* (red lines) mice. All *nob* mice tested behaved similarly (*n* = 9). (B) Two-second segments taken from the boxes in (A), on an expanded scale, show small-amplitude oscillating eye movements in *nob* (right) but not in wt (left) mice. These 2-s segments illustrate that wt mice made smooth eye movements in the presence of the moving contrast, whereas the eyes of *nob* mice oscillated in the horizontal direction. In both wt and *nob* mice, vertical eye movements were generally absent. (C) Power spectral density plots of the eye-movement velocity show an approximately 5-Hz oscillation frequency in *nob* mice (right) during moving and stationary stimuli, whereas the eyes of wt mice (left) did not oscillate under those conditions. The peak in the power spectrum for the moving stimulus (0.5 Hz) in wt results from stimulus-induced eye movements. (D) Relative power spectral density plots comparing *nob* eye movements (*n* = 9) in darkness (left panel), during vertical sine grating presentation (middle panel), and during horizontal sine grating presentation (right panel). A vertical grating with a spatial frequency of 0.1 cycles/deg effectively induced eye-movement oscillations, whereas a horizontal grating of the same spatial frequency did not. (E) The relation between spatial frequency and power of the eye-movement oscillations in the same mice. A spatial frequency of 0.1 cycles/deg was the most effective. Oscillating eye movements were absent in wt mice (*n* = 9). (F) Frequency-response plots of the OKR, tested by projecting a horizontally oscillating dot pattern (peak velocity of 18.85 deg/s) on a screen around the mouse. The eye-movement gain is expressed as the average velocity amplitude of the eye-movement response divided by the velocity amplitude of the stimulus. In wt mice (blue line; *n* = 11), the gain drops with increasing oscillation frequency. The eye-movement gain of *nob* mice (red line; *n* = 9) deviates from that of wt at low frequencies. Data in (D-F) are shown as mean ± SEM. The data underlying this figure can be found at https://figshare.com/account/home#/projects/65990. OKR, optokinetic response; wt, wild type.

https://doi.org/10.1371/journal.pbio.3000174.g001

By varying the spatial frequency and orientation of the stationary gratings, we determined that a vertical grating with a spatial frequency of 0.1 cycles/deg generated eye-movement oscillations with the strongest power (Fig 1D & 1E, red). Darkness and horizontally oriented gratings failed to induce significant eye-movement oscillations (Fig 1D). Additionally, no vertical oscillating eye movements were detected (green).

Because the *nyx* mutation affects signaling by retinal ON-BCs [8–11], we asked whether *nob* mice show changes in their retinal output. We recorded activity from GC axons in the optic nerve (Fig 2A) and found that *nob* GCs showed oscillating burst-spiking behavior with a mean frequency of 4.79 ± 0.13 Hz (n = 46) (Fig 2B and S2A Fig), which did not differ significantly from the mean frequency of their eye-movement oscillations (Student t test, t = −1.53, df = 61, p = 0.13). These oscillations were absent in wt GCs (Fig 2A & 2B). Because of the widespread oscillations across *nob* GCs, we hypothesized that the signaling of retinal image motion might be affected.

The direction of image motion is transmitted from the retina to the brain via two general pathways. ON-DSGCs, which are most sensitive to low temporal frequencies, low image velocities, and signal global motion project to the AOS [12–15] and are the primary neurons driving the optokinetic reflex [16]. In contrast, ON/OFF-DSGCs, which have a broad temporal frequency–response range, are mostly implicated in relative-motion detection and project mainly to the lateral geniculate nucleus (LGN) and superior colliculus (SC) [12–15]. To determine which of these two pathways is affected most in *nob* mice, we recorded the frequency-response curves of their eye movements induced by sinusoidally oscillating dot patterns with a constant peak velocity (Fig 1F). The frequency-response relation of *nob* (red symbols) and wt eye movements (blue symbols) differed, but only in the low frequency range, consistent with a malfunction in ON-DSGCs, suggesting that these GCs are predominantly involved in generating the nystagmus phenotype.

To test this idea, we recorded excitatory and inhibitory currents in *nob* ON-DSGCs, using *nob* mice crossed and backcrossed with SPARC-related protein-containing immunoglobulin domains 1 (SPIG1)$^+$ reporter mice in which ON-DSGCs coding for upward image motion are green fluorescent protein (GFP) labeled [17,18]. In contrast to wt ON-DSGCs, *nob* GFP$^+$ ON-DSGCs were visually nonresponsive, and both their excitatory and inhibitory currents oscillated with a mean frequency of 5.10 ± 0.22 Hz (n = 36) and 4.50 ± 0.38 Hz (n = 8), respectively (Fig 2C & 2D). The oscillation frequencies of *nob* eye movements, GC burst-spiking, and ON-DSGC excitatory and inhibitory currents did not differ significantly from each other (ANOVA: F = 1.320, df = 103, p = 0.272), indicating that a retinal oscillator, presynaptic to *nob* GCs, drives these oscillations (S2A Fig).

Using a multielectrode array (MEA), we recorded the activity of *nob* GCs extracellularly and assessed their light-evoked responses and oscillatory activity. *nob* ON-DGCs do not respond to light stimuli, and this makes it impossible to identify these neurons in MEA recordings. In the dark, about 55% (602 GCs; 10 retinas) of the *nob* GCs showed periodic variations in their autocorrelations (Fig 3A), indicating that they oscillated. We never observed such oscillations in wt GCs in either the dark or after a light flash (Fig 3Biv). To examine whether *nob* GCs oscillated synchronously, we selected nine oscillating *nob* GCs and, in the dark, aligned the activity of GC-2 through GC-9 such that their first spike in each of one hundred 2-s periods, spaced 3 s apart, corresponded with the first spike fired by GC-1 during the same period. The aligned traces were averaged (Fig 3Bi), and the averaged traces show that the spike patterns of GC-2 through GC-9 are unrelated to GC-1, indicating that their rhythmic firing differed in frequency and phase from the oscillations of GC-1. We also observed that the oscillations in the mean response of GC-1 reduced over time, suggesting that the frequency and phase of the spontaneous GC oscillations varied slowly over time. In contrast, a brief light flash synchronized oscillatory activity across all nine GCs (Fig 3Bii). In the light, their averaged traces of 100 repetitions showed clear oscillation patterns, indicating that light stimulation acted to phase-reset their activity and produced synchronized oscillations.

We found two clusters of *nob* GCs that oscillated in antiphase (Fig 3Biii). In one cluster, *nob* GCs responded initially to the light flash with a reduction in firing rate, identifying them
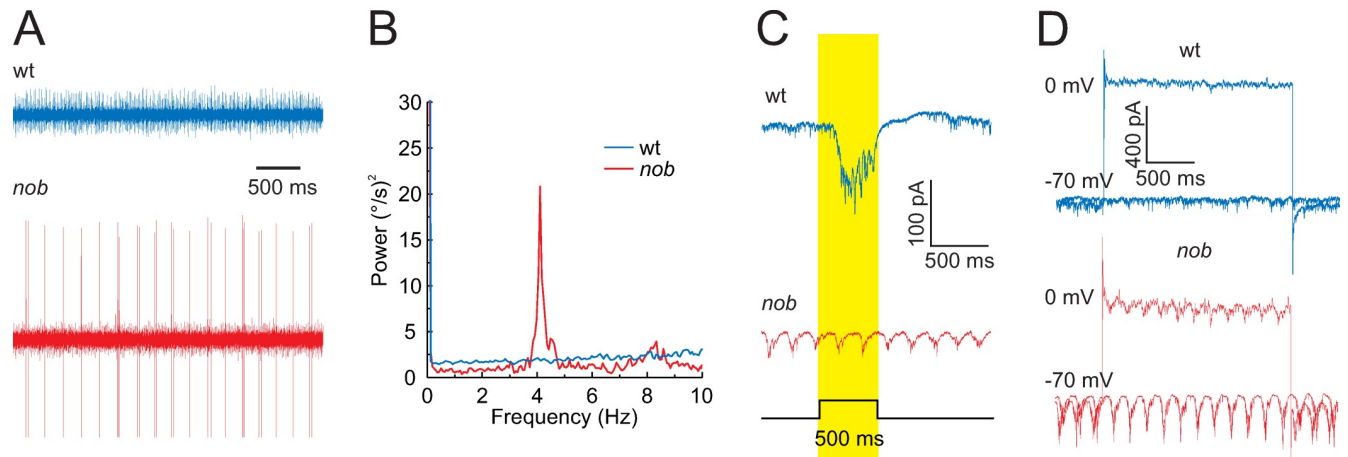
Fig 2. *nob* mice GC oscillate. (A) Optic nerve recordings of spontaneous GC spiking activity in wt and *nob* mice after 30 min of dark adaptation. The spontaneous activity of *nob* GCs shows oscillatory spiking patterns with a mean frequency of 4.79 ± 0.13 Hz ($n = 46$ isolated units). (B) In this example, the GC fundamental frequency is 4 Hz. (C) GFP-positive cells in wt/SPIG1+ mice show an increased inward current during a light flash, e.g., an ON response (blue trace). In *nob*/SPIG1+ mice, GFP-positive GCs lack a light-evoked inward current and show oscillating inward currents. (D) Inhibitory and excitatory currents in GFP-positive wt/SPIG1+ (blue) and *nob*/SPIG1+ (red) GCs recorded under voltage-clamp conditions (holding potential: 0 and −70 mV, respectively). In *nob* mice, both excitatory and inhibitory inputs oscillated with a mean frequency of 5.10 ± 0.22 Hz ($n = 36$) and 4.50 ± 0.38 Hz ($n = 8$), respectively. The data underlying this figure can be found at https://figshare.com/account/home#/projects/65990. GC, ganglion cell; GFP, green fluorescent protein; SPIG1, SPARC-related protein-containing immunoglobulin domains 1; wt, wild type.

https://doi.org/10.1371/journal.pbio.3000174.g002

as OFF-GCs. In the other cluster, GCs' mean firing rates remained unchanged during and after a light stimulation, suggesting they were ON-GCs, since all *nob* ON-GCs are visually unresponsive. During the light flash, the oscillatory activity of *nob* GCs synchronized within each cluster, as revealed by their short-time cross-correlations (Fig 3C). Both ON-GC/ON-GC and OFF-GC/OFF-GC pairs showed multipeak correlograms with a positive coefficient around zero lag time after light onset, indicating synchronized oscillatory firing. An ON-GC paired with an OFF-GC showed a similar multipeak correlogram but now had a negative correlation coefficient around zero lag time. This indicates that ON-GCs and OFF-GCs oscillate in antiphase. Fig 3D shows the mean cross-correlations for all ON-GC/ON-GC and OFF-GC/OFF-GC pairs and all the ON-GCs paired with all the OFF-GCs, before (blue) and during (red) the light flash. This behavior was found in all four retinas tested.

In the next series of experiments, we sought to establish a causal relationship between eye movements and GC oscillations in *nob* mice. First, we pharmacologically blocked or modified the excitatory inputs to the GCs and measured both GC oscillations and eye-movement oscillations. Blocking excitatory α-amino-3-hydroxy-5-methyl-4-isoxazolepropionic acid (AMPA) and N-methyl-D-aspartate (NMDA) inputs in vitro with a cocktail of 50 μM 6-Cyano-7-nitro-quinoxaline-2, 3-dione (CNQX) (50 μM 6, 7-dinitroquinoxaline-2,3-dione [DNQX]) and 10 μM D(−)-2-Amino-5-phosphonopentanoic acid (D-AP5) eliminated all *nob* GC oscillations (Fig 4Ai-iii). Similarly, intraocular injections of a similar cocktail in vivo eliminated eye-movement oscillations in awake and behaving mice (Fig 4Aiv). This shows that the eye-movement oscillations depend on retinal activity.

As functionally diverse GCs display oscillatory firing in *nob* mice (Fig 3B) [10], these oscillations presumably arise from a common presynaptic source. As we find two groups of *nob* GCs oscillating in antiphase (Fig 3B–3D), the AII amacrine cells (ACs) are a likely candidate for this presynaptic source, as they drive both ON- and OFF-GCs with opposite sign [19]. In mice with photoreceptor degeneration (retinal degeneration 1 [rd1] mouse), AII ACs generate intrinsic oscillations [20] that drive oscillatory firing of ON- and OFF-GCs in antiphase [21].
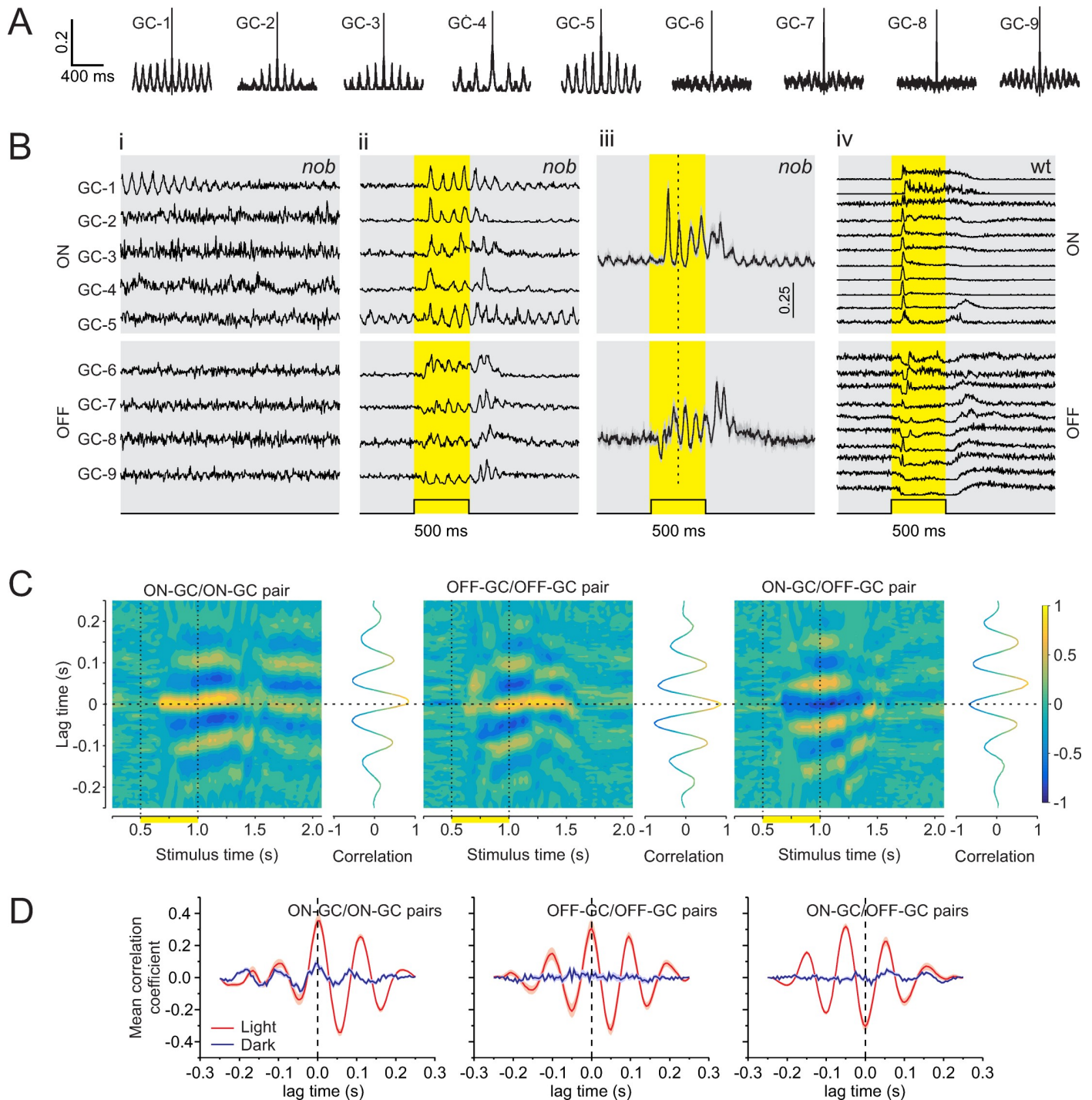
Fig 3. In the dark, *nob* mice GCs oscillate asynchronously, but light stimulation synchronizes their oscillations. Results based on GC spiking responses recorded on an MEA. (A) Autocorrelations of 9 representative *nob* GCs from one retina in the dark. Periodic variations in their autocorrelations indicate spontaneous oscillatory activity. (Bi) Each trace shows the mean normalized GC activity of 100 episodes of activity in the dark during the first 2 s of a 5-s window. All episodes were aligned to the first spike in the corresponding episode of GC-1 and then averaged. A clear oscillatory pattern is initially apparent for GC-1. In contrast, none of the other cells showed a similar pattern, suggesting that each *nob* GC oscillated with a frequency and/or phase, independent of GC-1. (Bii) Mean normalized activity of the same *nob* GCs in response to a 500-ms light flash (yellow shading). Note the presence of oscillation in all GCs, indicating that their phase was reset by the light flash. (Biii) Mean (± SEM) light-evoked oscillations of GCs could be separated into two clusters that oscillated in antiphase with each other. One cluster showed a decrease in spike rate just after light onset identifying them as OFF-GCs (bottom; *n* = 10), whereas the other cluster responded with a delay and in antiphase, suggesting they were ON-GCs (top; *n* = 13). (Biv) Mean responses of 21 wt GCs to the same stimulus used in (Bii-iii) show no oscillatory activity evoked by the light flash. (C) Short-time cross-correlations between mean responses of representative *nob* ON-GC/ON-GC, OFF-GC/OFF-GC, and ON-GC/OFF-GC pairs during the

same light stimulation. Line graphs flanking the heat maps (3D plots) show the cross-correlation for a time window of 250 ms, advancing in 25-ms steps. After light onset, and around zero lag time, peak-positive correlation coefficients are found for *nob* ON-GC/ON-GC and OFF-GC/OFF-GC pairs and peak-negative correlation coefficients for the ON-GC/OFF-GC pair. (D) Mean (± SEM) cross-correlations of all *nob* ON-GC/ON-GC (*n* = 78), OFF-GC/OFF-GC (*n* = 45), and ON-GC/OFF-GC (*n* = 130) pairs for *nob* GCs used in (Biii). Two time windows are illustrated. The blue line indicates a window immediately prior to light onset (250–500 ms); the red line indicates a window during the light flash (675–925 ms). Panels C and D show that the oscillations are poorly synchronized in the dark before the light flash and that light synchronizes the oscillations, which gradually dissipates again in the dark after the light flash. The data underlying this figure can be found at https://figshare.com/account/home#/projects/65990. GC, ganglion cell; MEA, multielectrode array; wt, wild type.

https://doi.org/10.1371/journal.pbio.3000174.g003

In these rd1 mice, the oscillation frequency of AII ACs can be decreased by blocking glycine receptors with the antagonist strychnine (STR) [20]. Similarly, in *nob* retina, application of 10 μM STR reduced both ON-DSGC oscillation frequency (control: 4.25 ± 0.12 Hz; STR: 2.67 ± 0.07; *n* = 6; paired Student *t* test, t = 5.27, df = 5, *p* = 0.003) (Fig 4Bi—iii) and the eye-movement oscillation frequency (control: 5.55 ± 0.05 Hz; STR: 2.83 ± 0.63; *n* = 3; paired Student *t* test, t = 7.30, df = 2, *p* = 0.018) (Fig 4Biv). Although 1 μM of STR already induced a reduction of the GC oscillation frequency of 0.92 ± 0.23 Hz (*n* = 3; *p* = 0.022), we used a higher concentration to induce a large and robust shift in oscillation frequency. This dose may have induced an additional block of GABA receptors as well. We used linopiridine hydrochloride (LP) to block the M-type potassium current [20] essential for the AII AC oscillations [22–24]. LP (30 μM) decreased the oscillation frequency of the ON-DSGCs from 5.71 ± 0.53 to 2.83 ± 0.40 Hz (*n* = 6; paired Student *t* test, t = 7.45, df = 5, *p* = 0.0007) and decreased the eye-movement oscillation frequency from 5.00 ± 0.00 to 1.75 ± 0.50 Hz (*n* = 3; paired Student *t* test, t = 6.48, df = 2, *p* = 0.023) (Fig 4C).

Finally, we disrupted the gap-junction coupling between the ON-BCs and the AII AC network [25–27]. In rd1 mice, the gap-junction blocker meclofenamic acid (MFA) blocks the oscillations of the AII ACs [21,28]. MFA (100 μM) blocked the oscillation in GCs (Fig 4Di-iii) in *nob* mice, corroborating the evidence for AII ACs being the source of the oscillations. As the gap junctions themselves are composed of connexin 36 (Cx36), we crossed Cx36 knockout mice and *nob* mice. In these *nob* mice lacking Cx36, both the GC oscillations and the eye-movement oscillations were absent (Fig 4D).

For extended statistics of these pharmacological experiments, see S2B Fig. Together, the results of Fig 4 indicate that (1) the oscillator driving the oscillating eye movements is located in the retina, (2) the AII ACs are critically involved in generating the oscillations in *nob* GCs, and (3) there is a causal relation between the *nob* GC oscillations and their eye-movement oscillations.

Discussion

This study reveals—for the first time, to our knowledge—a pathophysiological mechanism for a specific form of congenital nystagmus and shows that its origin is retinal. We propose the following mechanism (Fig 5A & S3 Fig). In wt mice, ON-DSGCs, which are sensitive to low-velocity global image motion, respond coherently when an image moves across the retina. Their coherent output reflects the direction and speed of global image movement: i.e., the retinal slip signal. This signal forms the input to the AOS, where it induces compensatory eye movements that stabilize the image on the retina. In *nob* mice, the network behaves quite differently. *nob* ON-DSGCs are nonresponsive to light stimuli and thus cannot detect image motion, which may underlie the lack of a well-developed optokinetic response (OKR). In addition, *nob* GCs oscillate spontaneously, which, as shown in this paper, induces a pendular nystagmus.

We propose that the origin of these oscillations is the AII ACs for the following reasons. Firstly, the source of the oscillations is presynaptic to GCs. Secondly, AII ACs contain an
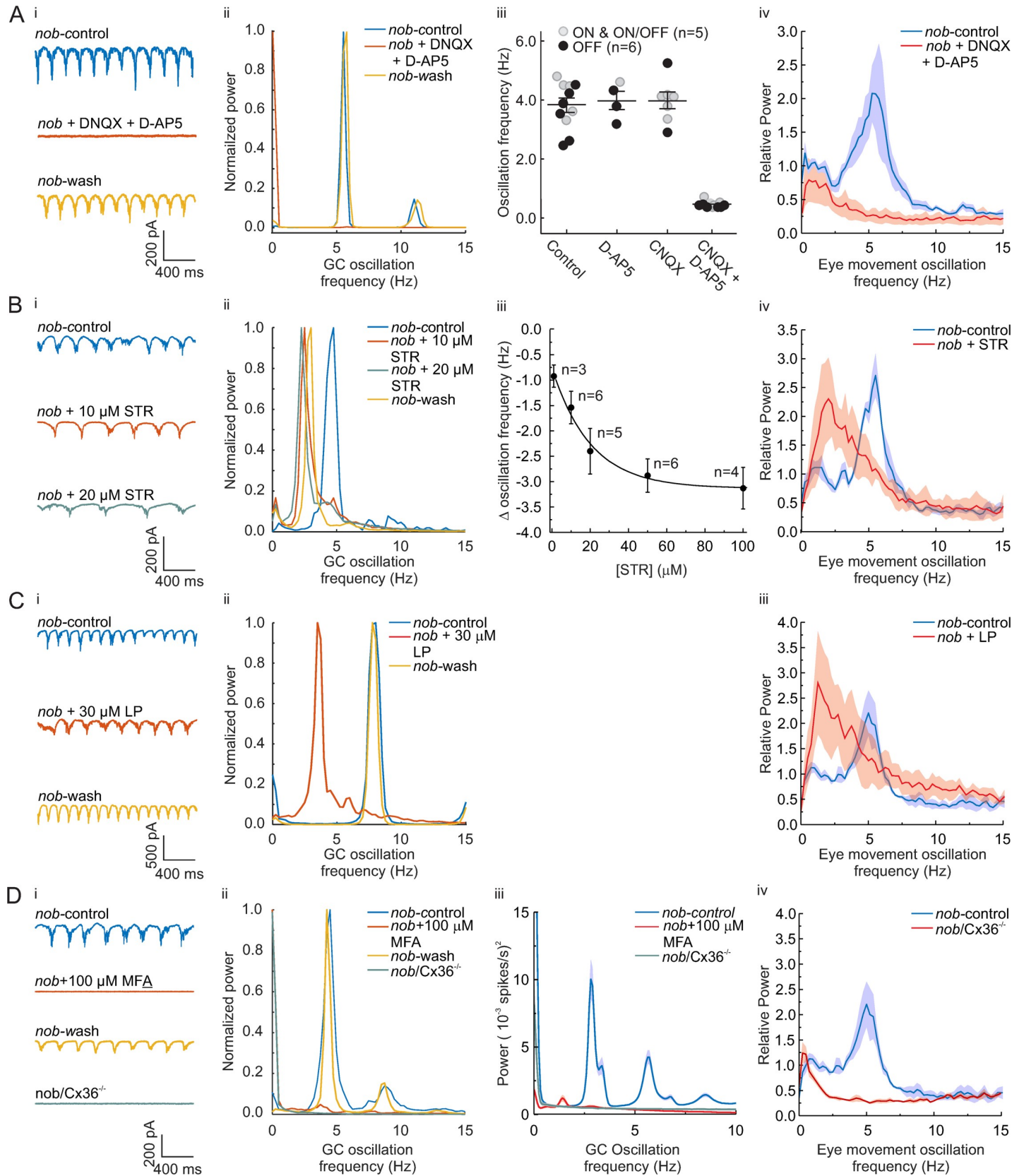
Fig 4. Pharmacological block of excitatory and inhibitory inputs in *nob* retina blocks or modify both GC and eye-movement oscillations. (Ai) Oscillating excitatory currents of *nob* ON-DSGCs (top) are blocked by a cocktail of 50 μM DNQX and 10 μM D-AP5 (middle) and return after washout (bottom). (Aii) The power spectral density plot of the data in (Ai) shows that DNQX/D-AP5 eliminates the 5-Hz oscillating excitatory current. This was found in all *nob* GCs tested (*n* = 5). (Aiii) CNQX or D-AP5 administered separately do not block excitatory current oscillations, whereas their combination blocks excitatory current oscillations in *nob* ON-, OFF-, and ON/OFF-GCs and displaced ACs. (Aiv) Oscillating eye movements in awake *nob* mice (*n* = 5) are blocked by intravitreal injections of DNQX/D-AP5 (red; control: blue). (Bi and Bii) STR reduces the oscillation frequency of *nob* ON-DSGCs excitatory currents. (Biii) Mean data (± SEM) shows that STR consistently reduced the oscillation frequency in a dose-dependent manner. (Biv) Mean (± SEM) power spectral density plots (*n* = 3) show that intraocular injection of STR reduced the eye-movement oscillation frequency in *nob* mice. (Ci) Bath application of LP reduced the oscillation frequency of *nob* ON-DSGCs excitatory currents. (Cii) The power spectral density plots of the ON-DSGC, shown in (Ci), show a shift in peak oscillation frequency to lower frequencies. This was found in all *nob* GCs tested (*n* = 6). (Ciii) Mean (± SEM) power spectral density plots (*n* = 3) show that intraocular injection of LP reduced the frequency of oscillating eye movements in *nob* mice. (Di) Bath application of MFA blocks the oscillations of *nob* ON-DSGCs excitatory currents and oscillations are absent in *nob/Cx36⁻ᐟ⁻* animals (green trace). (Dii) The power spectral density plots of the ON-DSGC, shown in (Di), show the blocking of oscillations (red trace). This was found in all *nob* GCs tested (*n* = 6). Oscillations were absent in all 7 *nob/Cx36⁻ᐟ⁻* animals tested. (Diii) Mean (± SEM) power spectra of the spiking activity of *nob* GCs recorded on the MEA in control (blue trace *n* = 90) and 100 μM MFA (red trace, *n* = 98) conditions and in *nob/Cx36⁻ᐟ⁻* GCs (green trace, *n* = 56). (Div) Mean (± SEM) power spectral density plots (*n* = 3) show that *nob/Cx36⁻ᐟ⁻* mice do not show oscillating eye movements. All GC recordings were done in the dark. For the experiments shown in (Aiv, Biv, Ciii, and Div), the stimulus was a stationary sinusoidal grating with a spatial frequency of 0.1 cycles/deg and 100% contrast. The data underlying this figure can be found at https://figshare.com/account/home#/projects/65990. AC, amacrine cell; CNQX, 6-Cyano-7-nitroquinoxaline-2, 3-dione; *Cx36*, connexin 36; GC, ganglion cell; D-AP5, D(−)-2-Amino-5-phosphonopentanoic acid; DNQX, 6, 7-dinitroquinoxaline-2,3-dione; LP, linopiridine hydrochloride; MEA, multielectrode array; MFA, meclofenamic acid; ON-DSGC, ON direction-selective GC; STR, strychnine.

https://doi.org/10.1371/journal.pbio.3000174.g004

intrinsic, membrane-potential dependent oscillator, consisting of a fast sodium channel, and both a fast and a slow (M-type) potassium channel [20]. When the AII AC membrane potential is outside its normal working range because of altered input from the ON-BCs, the AII ACs start to oscillate [20]. Finally, the oscillations of ON- and OFF-GCs are driven in antiphase, which AII ACs will do, since they drive ON- and OFF-GCs with opposite sign.
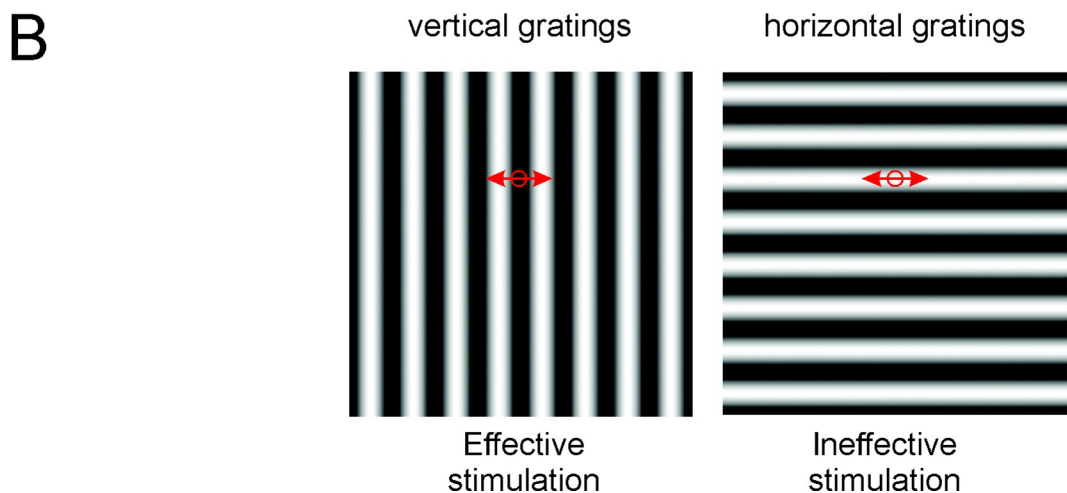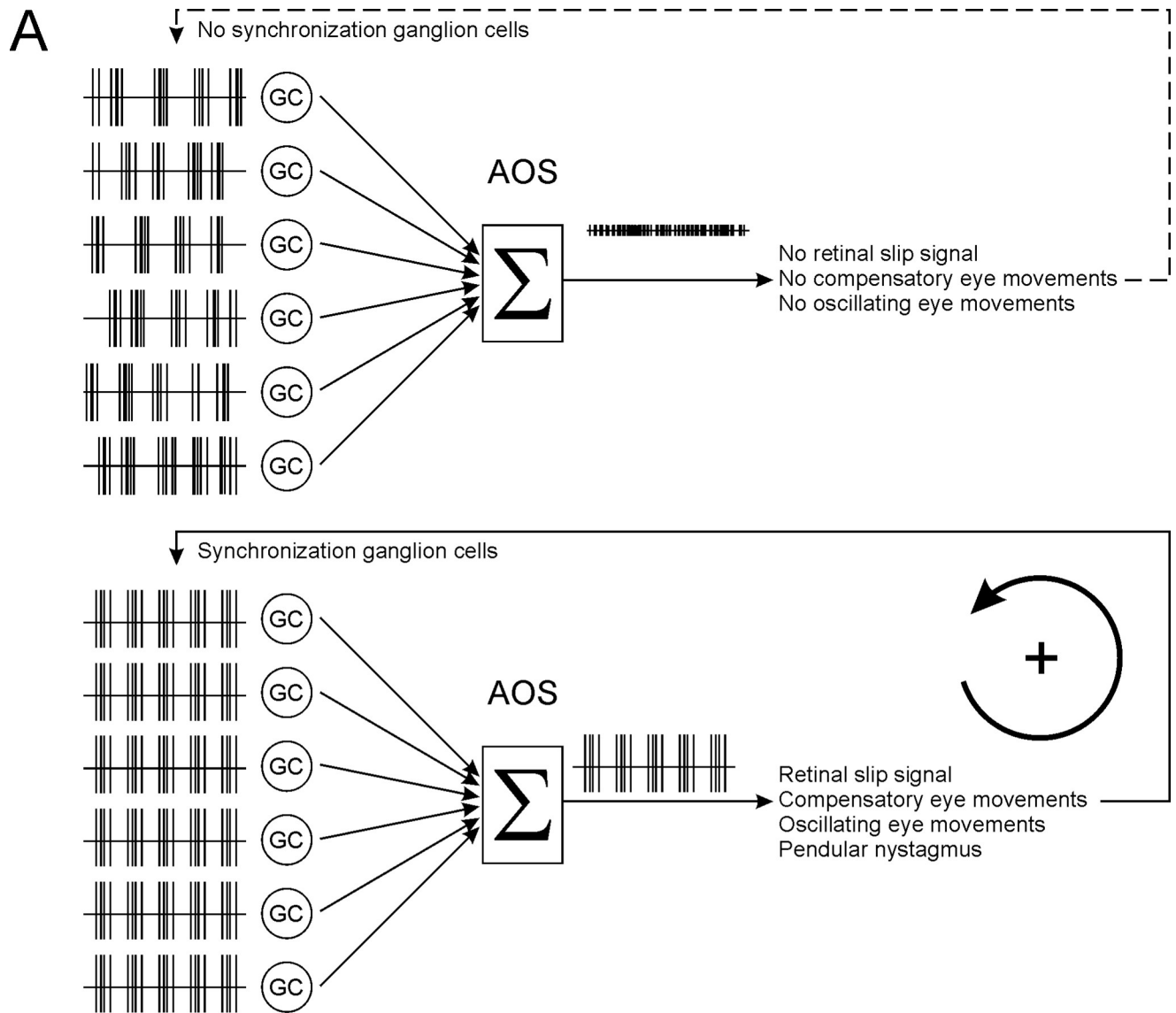
How could light stimulation synchronize the oscillations in the GCs? Since the oscillator in AII ACs is an intrinsic feature of the AII ACs, they could oscillate rather independently of each other, leading to asynchronous GC oscillations, as we find in the dark. We hypothesize that global light stimulation depolarizes the membrane potential of the AII ACs by crossover inhibition driven by GABAergic OFF ACs [29]. This will phase-reset and synchronize the AII ACs and subsequently synchronize in antiphase both the ON- and OFF-GCs they project to.

The consequence is that despite the absence of a classical visually evoked response in *nob* ON-DSGCs, their oscillations synchronize when the retina is stimulated with a global light stimulus. The combined activity of the synchronized oscillating *nob* ON-DSGCs is interpreted in the AOS as an oscillating retinal slip signal, and, in response, oscillating compensatory eye movements are generated: pendular nystagmus. On the other hand, when the oscillations of *nob* ON-DSGCs are asynchronous, such as in the dark, the integrated output to the AOS will not oscillate and will not evoke a pendular nystagmus.

Once initiated, oscillating eye movements over an image induce retinal activity that phase resets the retinal oscillator (AII ACs) and maintains the synchronous oscillations of ON-DSGCs and pendular nystagmus (Fig 5A). This represents a self-maintaining loop. Consistent with this idea, a horizontally oriented grating fails to induce oscillating eye movements, because horizontal eye movements over a horizontal grating appears as a stationary stimulus to GCs (Fig 5B). This will not modulate retinal activity and will not synchronize GC oscillations, and pendular nystagmus is absent (Fig 1D).

Although we suggested that the ON-DSGCs drive the oscillating eye movements, we cannot exclude contribution of other GCs. However, ON-DSGCs are the most important GCs to detect the direction of global retinal image motion that is used as a retinal slip signal by the AOS to induce compensatory eye movements [16]. Oscillations in these cells will therefore be especially effective in inducing oscillating eye movements.

The suggestion that AII ACs are the source of the oscillations implies that all ON-DSGCs oscillate. If this is the case, why is nystagmus in the CSNB patients and *nob* mice only horizontal when ON-DSGCs are tuned for image movement in three directions: naso-temporal,

A

No synchronization ganglion cells

AOS

Σ

No retinal slip signal
No compensatory eye movements
No oscillating eye movements

Synchronization ganglion cells

AOS

Σ

+

Retinal slip signal
Compensatory eye movements
Oscillating eye movements
Pendular nystagmus

B

vertical gratings   horizontal gratings

Effective   Ineffective
stimulation   stimulation

Fig 5. Model for the generation of night blindness–associated congenital nystagmus. (A) wt ON-DSGCs ("GC") signal direction of global image motion to the AOS. In the AOS, the ON-DSGC signals are integrated ("Σ"), and a compensatory eye movement is induced. In the dark, *nob* ON-DSGC spiking activity oscillates, but these oscillations are asynchronous. The integrated inputs to the AOS from asynchronous oscillating *nob* ON-DSGCs do not generate a signal sufficient to trigger an eye movement. In the presence of a stimulus-containing contrast, the oscillations of *nob* ON-DSGCs are synchronized, and their integrated input to the AOS oscillates, representing a significant retinal slip signal, and hence, a compensatory eye movement is induced. This eye movement will evoke a light response and keeps the GCs synchronized. The result is a pendular nystagmus. (B) A vertical grating oscillating horizontally over the retina effectively activates GCs, since the stimulus changes within the receptive field of the GC (circle) and keeps the GCs synchronized. A horizontal grating oscillating horizontally over the retina is ineffective in inducing a response in retinal neurons, since the stimulus will not change within the receptive field of the neurons (circle) and hence GCs will not be synchronized and thus no pendular nystagmus will occur. AOS, accessory optic system; GC, ganglion cell; ON-DSGC, ON direction-selective GC; wt, wild type.

https://doi.org/10.1371/journal.pbio.3000174.g005

upward, and downward [14]? One of the simplest explanation is that the retinal slip signals generated by synchronously oscillating ON-DSGCs tuned for upward and downward motion cancel each other. This can occur, for instance, at the neuronal level of the vestibular oculomotor nuclei or possibly even at the level of the eye muscles. In contrast, the naso-temporal signal is not canceled, as there is no, or only a few, opposing ON-DSGCs [14].

In the present paper, we discuss the origin of a specific form congenital nystagmus, i.e., spontaneous small-amplitude involuntary oscillating eye movements. This pathological condition is distinct from the OKR, in which the eyes follow the global movement of the stimulus followed by a fast reset saccade. The OKR, sometimes referred to as optokinetic nystagmus, is often reduced or absent in nystagmus patients. However, the conclusion that congenital nystagmus arises as a consequence of a mere absence of the OKR is unwarranted, since, for example, mice with mutations in FERM domain-containing protein 7 (FRMD7) [30] have no horizontal OKR but do not develop a pathological nystagmus.

It has been suggested that congenital nystagmus originates from a disruption in the interaction of the subcortical optokinetic pathways (AOS) and cortical foveal pursuit system [1]. However, our findings show that the cause of congenital nystagmus associated with CSNB lies within the retina in the afoveate mouse. Since the optokinetic systems of afoveate and foveate animals differ, generalizing our findings in *nob* mice to humans with CSNB requires caution. That said, given the balance of our results, we proposed that the *nob* mouse model is relevant to human CSNB patients for the following reasons. Firstly, the nystagmus in young CSNB patients (S1 Fig) and *nob* mice is identical (Fig 1). Secondly, the photoreceptor to ON-BC synapse is highly conserved across mammals and even across vertebrates [31]. Thirdly, mutations in proteins specific for this synapse lead to the same CSNB phenotype in mice and humans [32], suggesting similar underlying retinal mechanisms. Fourthly, starburst amacrine cells (SACs), which are fundamental for generating direction-selective responses of GCs [30] and DSGCs [33], are found both in mouse and primate retina [34]. Finally, retrograde tracing experiments reveal retinal projections to the AOS in both mice and primates [35].

From a therapeutic point of view, our results suggest that the primary pathogenic condition in patients with this form of congenital nystagmus occurs in the retina in the form of synchronized oscillations of GCs. Therapeutic interventions aimed at desynchronization of the oscillating GCs in the retina may serve to reduce or eliminate the nystagmus.

Material and methods

Animals

All animal experiments were carried out under the responsibility of the ethical committee of the Royal Netherlands Academy of Arts and Sciences (KNAW), acting in accordance with the European Communities Council Directive of 22 July, 2003 (2003/65/CE), or the University of Louisville Animal Care and Use Committee. All experiments we conducted under license

number AVD-801002016517, issued by the Central Comity Animal Experiments of the Netherlands, and under the license number 17763, issued by the University of Louisville Animal Care and Use Committee.

wt mice, *Mus musculus*, were obtained from Janvier labs. *Nob* and *Cx36* knockout mice were obtained from the McCall lab (University of Louisville, Louisville, KY, United States), and SPIG1+ mice were obtained from the Noda lab (National Institute for Basic Biology, Okazaki, Japan). *Nob*/Spig1+ and *Cx36* knockout mice were crossbred to accomplish a double knockout with labeled ON-DSGCs. Since the *nob* mutation is X-linked, only male animals were used. For wt SPIG1+, both male and female animals were used. All mice were kept in a C75BL/JRj background. The age of the animals ranged from 4 wk to 1 y.

Eye-movement recordings

Surgical preparation.   Prior to the start of experiments, adult animals were equipped with a head-fixation pedestal, an aluminum bit with an integrated magnet, attached to the parietal bones of the skull using dental cement (Super Bond, Sun Medical). Surgery was performed under general isoflurane/O_2 anesthesia and topical anesthesia (bupivacaine). Analgesia was offered by subcutaneous injection of metacam (2 mg/kg). The recovery time was at least 2 d after pedestal surgery. During experiments, the animal was placed head-fixed in the experimental setup using a custom-made adapter, which allowed panoramic vision.

Optokinetic stimulator.   For the optokinetic experiments, two experimental setups were used. In the first system, a modified Marquee 9500 CRT projector (100 fps) generated a large panoramic visual surround (545 nm) onto three large back-projection screens (1.47×1.18 m; Stewart Filmscreen) that were placed around the animal to create a combined field of view of $270° \times 77.5°$. The average luminance of the visual stimulus was 10 cd/m^2. Mickelson contrast of the grating stimuli was about 90%. In the second setup, two Benq XL2420t high-performance monitors (120 fps, gamma-1.745) were placed in V-formation around the animal, and the closest distance between the screen surface and the mouse head was 16.5 cm. Screen dimensions were 56.9×33.8 cm (combined field of view: $240° \times 50°$). Mickelson contrast of the grayscale grating stimuli approached 100%. The average luminance of the sine grating stimuli was 71.6 cd/m^2. For measurements in darkness, the displays were switched off. Visual stimuli consisted of sine wave gratings, homogeneous grayscale images, and dotted patterns (dot radius 1°, center-to-center distance 5.35°). All stimulus patterns were computer generated and corrected for perspective distortion by projection onto a virtual sphere centered on the animal's head.

Eye-movement recordings.   Eye movements were recorded using an infrared video tracking system (JAI RM-6740CL monochrome CCD camera, 200 fps). In a few instances (Fig 1A–1C), pilocarpine (2%) eye drops were used to reduce pupil dilatation. A 2D eye position was computed from the relative distance between pupil center and corneal reflections of the infrared LEDs [36] and pupil size [37,38]. Epochs containing saccades, eye blinks, and motion artifacts were excluded from analysis. Eye velocity was smoothed using a Gaussian smoothing kernel with a SD of 7.5 ms (25-Hz cutoff). For monocular visual stimulation (Figs 1D, 3Aiv, 3Biv and 3Ciii), a miniature blackout cap was placed over the contralateral eye.

Intraocular injections.   Intravitreal injections were administered under brief isoflurane/O_2 sedation and topical anesthesia applied to the injection spot (0.4% oxybuprocaine). The eye movements were measured after the mouse recovered completely from the anesthesia. We used injection volumes ranging between 1 and 3 μL. To block AMPA receptors, we used either DNQX (Tocris, 50 μM final concentration) or CNQX (Tocris, 50 μM final concentration). CNQX and DNQX were assumed to act equally. To block NMDA receptors, we used D-AP5

(Tocris, 10 μM final concentration). To block glycinergic inhibition, we used STR (about 10 μM final concentration). The high dose of STR might have blocked GABA receptors as well. To block the M-type K current, we used LP (Tocris, 30 μM final concentration). Drugs were dissolved in Hank's Balanced Salt Solution (Sigma-Aldrich).

Analysis of eye-movement recordings.   PSDs were computed from angular eye velocity using Welch's method with a 4-s window length, 75% overlap between windows, and a Hann window function. The fundamental frequency was computed by weighted averaging the frequencies with a magnitude $> 90\%$ of the maximum power in the PSD. For comparisons between different stimulus conditions in *nob* mice, PSDs were normalized to the average power ≤ 2 Hz.

In vivo optic nerve recordings

Surgical preparation.   All surgical procedures were performed at light-adapted levels and have been published previously [39,40]. Briefly, anesthesia was induced with an intraperitoneal injection of a Ringer's solution containing ketamine and xylazine (127 and 12 mg/kg). Anesthesia was maintained with supplemental subcutaneous injections (about every 45 min) of anesthetic at 50% of initial concentration. The head was secured in a stereotaxic frame (David Kopf Instruments, Tujunga, CA, USA), a craniotomy was performed, and the overlying cortex was removed to expose the optic nerve. Throughout the experiment, body temperature was maintained at 37°C with a feedback-controlled heating pad (TC-1000; CWE, Ardmore, PA, USA). Topical phenylephrine hydrochloride (2.5%) and tropicamide (1%) ophthalmic solutions were applied to dilate the pupils and paralyze accommodation. Clear zero-powered lenses [41] moistened with artificial tears kept the cornea from drying. At the end of the experiment, animals were euthanized with an overdose of anesthetic followed by cervical dislocation.

Extracellular GC axon recordings.   Action potentials were recorded extracellularly from single optic nerve axons using sharpened tungsten microelectrodes (impedance = 30–100 MΩ). A reference electrode was inserted subcutaneously. Action potentials from single GC axons were isolated, amplified (X3+Cell; FHC, Bowdoinham, ME, USA), digitized at 15 kHz (Power1401, Cambridge Electronic Design, Cambridge, United Kingdom), and stored for offline analysis. Isolated spike trains were simultaneously displayed on an oscilloscope and computer monitor and played over an audio monitor to obtain direct feedback of the cell's response to visual stimuli. Responses were analyzed offline using Spike2 software v4.24 (Cambridge Electronic Design, Cambridge, United Kingdom). Spikes were accumulated within a 50-ms bin width and displayed as poststimulus time histograms (PSTHs). Each average PSTH was smoothed by fitting it with a raised cosine function with a 50-ms smoothing interval to minimize alteration of the peak firing rate and maximize signal-to-noise ratio [39].

Recording and analysis of GC spontaneous activity.   Spontaneous activity was determined for GCs in the dark over durations up to 200 s. The presence of a rhythmic component in the spontaneous activity was assessed using a fast Fourier transform (FFT) that produced a power spectrum (Spike2 4.24; Cambridge Electronic Design, Cambridge, UK). A peak fundamental frequency was considered significant if its power was three standard errors (SEs) above the mean power between 0.5 and 30 Hz [42]. To estimate the consistency of the rhythmic activity, the recorded spontaneous activity was divided into segments of 20 s, and FFTs were performed on each segment to identify the fundamental peak. The mean fundamental frequency and its SE were computed across all segments.

MEA recordings of GCs

Mice were dark-adapted for at least 1 h, euthanized with a mixture of CO_2/O_2, and cervically dislocated. Under dim red light, the eyes were removed and placed in oxygenated Ames

medium. The eyecup was prepared by removing the cornea, lens, and as much vitreous humor as possible. Using a fine forceps, the retina was carefully dissected away from the sclera. Small incisions were made to flat-mount the retina. Regardless of whether the isolated retinas were used in the MEA recordings or for whole-cell patch clamp recordings, they were continuously superfused with Ames' medium or Ringer's solution and gassed with a mixture of O_2 and CO_2 at pH of 7.4 and 29–36˚C.

Recording of MEA data.   Isolated retinas were placed photoreceptor side up on a perforated 60 electrode array (60pMEA200/30iR-Ti using a MEA2100 system: Multichannel systems, Reutlingen, Germany) in a recording chamber mounted on an Nikon Optiphot-2 upright microscope and viewed under IR with an Olympus 2x objective and video camera (Abus TVCC 20530). Extracellular multiunit GC activity was recorded at 25 kHz in MC rack (Multichannel systems, Reutlingen, Germany), zero-phase bandpass filtered (250–6,250 Hz) with a fourth-order Butterworth filter in Matlab (MathWorks, Natick, MA, USA), and sorted into single-unit activity with "offline spike sorter" (Plexon, Dallas, TX, USA). Spikes were detected using an amplitude threshold $> 4\sigma_n$ where σ_n is an estimation of the background noise

$$\sigma_n = median\left\{\frac{|x|}{0.6745}\right\}$$

with x being the bandpass-filtered signal [43]. The detected spikes were manually sorted into single units based on principal component or amplitude variables versus time. The clustering versus time approach allowed us to track changes in extracted features of single units occurring over extended recording periods and with differing firing rates.

Optical stimulator.   Light stimuli were generated with Psychophysics Toolbox Version 3 [38]. Stimuli were projected onto the retina from the photoreceptor side by a DLP projector (Light Crafter 4500, Wintech, Carlsbad, CA, USA) using a custom-built 2x water immersion objective. One pixel of the DLP projector had a size on the retinal surface of 2.1 μm. Only white light stimuli were used. The "dark" light intensity was 6 μW/m^2, and the maximal "light" intensity was 176.2 μW/m^2.

Analysis of MEA data.   For MEA recordings, rhythmic components in the spontaneous activity were assessed using single-unit activity during 600 s of darkness. Spike trains were binned into 1-ms intervals and then divided into 5-s nonoverlapping periods. Each segment was baseline subtracted, and the PSD and autocorrelation were evaluated over 120 segments, which were then averaged. The autocorrelations were normalized such that they were equal to 1 at zero lag. PSD was estimated by Welch's modified periodogram using 4-s windows, with 75% overlap, multiplied by a Hamming window function, and a 4-s discrete Fourier transform length.

Synchronized firing between units was assessed by cross-correlation after stimulation with a full field light stimulus presented for 500 ms. The flash was preceded and followed by a 500- and 1,000-ms period of darkness. Individual-unit spike trains were binned into 5-ms interval, and the response to 100 repetitions was averaged. The mean responses were divided into 250-ms windows, detrended, and then cross-correlated. For short-time cross-correlations, a 250-ms window was used that advanced in 25-ms steps.

Voltage-clamp recordings of GCs

Whole-cell voltage-clamp recordings were performed from GFP-labeled GCs in retinas mounted (GC side up) in a recording chamber (Warner Instruments, Hamden, CT, USA). The recording chamber was mounted on a Nikon Eclipse E2000FN microscope (Nikon,

Tokyo, Japan) and viewed with a Nikon 60x water immersion objective with infrared differential interference contrast and a video camera (Philips, Eindhoven, the Netherlands). The GFP-labeled cells were identified using a short flash of 450–490 nm light.

Solutions. Ames' medium supplemented with 1.9 g/L of $NaHCO_3$ was used as the external bath solution, and whole-cell patch pipette solution contained [mM] 112 Cs-Methanesulfonate, 8 CsCl, 10 EGTA, 10 HEPES, 2 ATP-Mg, and 0.3 GTP-Na3, pH adjusted to 7.2 with CsOH, ECl = −69.92 mV, except for data shown in Fig 4Aiii. Here, we used a bicarbonate buffered Ringer's bath solution containing [mM] 125 NaCl, 2.5 KCl, 1 $MgCl_2$, 1.25 NaH_2PO_4, 20 glucose, 26 $NaHCO_3$, and 2 $CaCl_2$ and a whole-cell patch pipette solution containing [mM] 120 Cs-gluconate, 1 $CaCl_2$, 1 $MgCl_2$, 10 Na-HEPES, 11 EGTA, 4 ATP and 1 GTP, and 1% LY. In these experiments, freshly prepared CNQX (Tocris) or DNQX (Tocris), D-AP5 (Tocris), and STR were added to the bath solution to block AMPA, NMDA, and glycine receptors, respectively. CNQX and DQNX were assumed to act equally. A cocktail of 50 μM DNQX and 10 μM D-AP5 in the external bath solution was prepared freshly before the experiment. For the dose-response curve of STR, the following concentrations were used: 1, 10, 20, 50 and 100 μM STR. Chemicals were obtained from Sigma-Aldrich (St. Louis, MO, USA) unless otherwise indicated.

Optical stimulator. Light stimuli were generated with Psychophysics Toolbox Version 3 [38]. Light stimuli were projected onto the retina from the photoreceptor side by an Acer C20 picoprojector via the microscope condenser. One pixel of the projector had a width of 4.8 μm on the retinal surface. The "dark" light intensity was 0.3 cd/m^2, and the maximal "light" intensity was 450 cd/m^2.

Recording equipment. Whole-cell data were recorded with a HEKA EPC10 patch clamp amplifier using PatchMaster software. The data were sampled at 10 kHz and filtered at 5 kHz with a four-pole Bessel low-pass filter. In a second setup, data were collected with a Multiclamp 700B amplifier using Digidata 1322A digitizer (MDS Analytical Technologies, Union City, CA, USA) and Clampex 10.2 software (MDS Analytical Technologies, Union City, CA, USA) to generate command outputs, trigger the light stimulus, and acquire and analyze analog whole-cell voltages. These data were sampled at 10 kHz and filtered at 2.4 kHz with a four-pole Bessel low-pass filter. Matlab (MathWorks, Natick, MA, USA) and Igor.pro (WaveMetrics, Portland, OR, USA) were used to analyze the data.

Statistics

Statistical analyses were performed using Origin Pro 8 (Northampton, MA, USA) or Matlab (MathWorks, Natick, MA, USA). All mean values are presented ± SEM. Statistical significance was tested using a (paired) Student t test or a one-way ANOVA. Normality was tested using the Shapiro-Wilk test. The distribution of the frequencies of the eye movements (df = 17, $p = 0.28$), the GCs optic nerve recordings (df = 46, $p = 0.71$), and the GC excitatory currents (df = 38, $p = 0.26$) were normally distributed. Differences with $p < 0.05$ were considered statistically significant.

Supporting information

S1 Fig. Eyes of CSNB patients oscillate horizontally at 6 Hz. The patients studied by Simonsz and colleagues [3] had horizontal pendular nystagmus combined with tonic downgaze and a low-frequency, upgaze-evoked nystagmus. Although the tonic downgaze disappeared at 2–3 y of age, the horizontal nystagmus remained. We quantified the nystagmus of three patients (age: 3.5, 3.5, and 5 y) whose video material was of sufficient quality. The original UMATIC video movies were digitized, and the digital clips were stabilized and aligned using the

compositing program Nuke (The Foundry, London, UK). The nasal corner of the eye and the surrounding area were used as references for the stabilization. After stabilization of the movie, a circle with a fixed diameter the size of the iris was fitted through the iris (see S1 Movie). The coordinates of the center of the circle were used as measure for the eye position, and the resulting time series of eye positions were Fourier transformed using Matlab. No attempt was made to calibrate the amplitude of the oscillations, and hence, the amplitudes are given in pixels. (Ai) Total horizontal (blue) and vertical (red) eye movements of patient #1 in pixels. Large-amplitude horizontal and vertical eye movements occurred, as the children could shift their gaze freely. On top of these large-amplitude eye movements, small-amplitude oscillations are visible only for the horizontal eye movements, which is also evident in the power spectrum (Aii). There are two peaks visible in the power spectrum: one broad peak below 2 Hz and one narrow peak around 7 Hz. The low-frequency component results from gaze shift. The two components were separated by calculating the moving average over a window of 5 frames (Bi) and subtracting this average from the original traces (Ci). The power spectra of these two components are shown in Bii and Cii. For each patient, four separate episodes were analyzed, and the episodes selected do not contain eye blinks. (D) The power spectra of the horizontal eye movements of the individual episodes per patient. All traces show peaks in the range of 5–8 Hz. (E) The mean power spectra per patient. (F) Box plots of the oscillation frequency for the various video clips for each patient. The oscillation frequencies across the various patients did not differ significantly (ANOVA: F = 3.75, df = 11, p = 0.06), and the mean peak oscillation frequency over all patients was 6.25 ± 0.63 Hz (n = 3) (age range: 3 mo–3 y). This oscillation frequency is considerably lower than the 10–20 Hz reported by Pieh and colleagues in a patient population that included the same patients as described by Simonsz and colleagues [3,44] and analyzed in this paper. Since Pieh and colleagues [45] did not disclose the methods of how the eye movements were analyzed, it remains puzzling why their estimated eye-movement oscillation frequency differs so much from ours. We complied with relevant ethical regulations applicable to clinical eye-movement recording at the time. Patient data: The three video recordings of the children aged 0–3 y were made in 1990 and 1992 in the Kantonsspital St. Gallen, Switzerland, as a clinical recording of eye movements in the course of their diagnostic work-up and treatment by their treating ophthalmologist (HJS). All clinical investigations have been conducted according to the principles expressed in the Declaration of Helsinki. Informed consent for publication of the video recordings of the eye movements of the patients had previously been obtained from the parents. Renewed written permission to publish the video material was obtained from the patients themselves, who are now adults. The data underlying this figure can be found at https://figshare.com/account/home#/projects/65990.
(EPS)

S2 Fig. Statistical data of the GC and eye-movement oscillation frequencies. The black open square indicates the mean of all results, the box indicates the interquartile range (25%–75%), the vertical lines indicate the 5%–95% range, and the colored circles indicate the individual data points. (A) Box plots of all measurements in control conditions. (B) Box plots of all pharmacological experiments for both the GC oscillations and the eye-movement oscillations. The data underlying this figure can be found at https://figshare.com/account/home#/projects/65990. GC, ganglion cell.
(EPS)

S3 Fig. Schematic diagram of the wiring of BCs, AII ACs, SACs, and ON-DSGCs. wt retinal circuit (top panel) compared to the *nob* retinal circuit (bottom panel). wt rod ON-BCs provide an excitatory input to AII ACs. AII ACs are electrically coupled with each other and to cone ON-BCs, and they provide a glycinergic inhibitory input to cone OFF-BCs. Cone ON- and

OFF-BCs provide a direct excitatory input to ON- and OFF-GCs. The pathway from rod > rod ON-BC > AII ACs > GCs is the primary rod pathway. AII ACs also receive a glycinergic inhibitory input. ON-DSGCs receive excitatory input from cone ON-BCs and are inhibited by ON-SACs. The interaction between ON-BC excitation and ON-SACs inhibition produces direction-selective responses in ON-DSGCs. OFF-BC excitatory input to AII ACs is relayed to cone ON-BCs via electrical coupling as well as via crossover inhibition between the ON and OFF pathways. In *nob* retina, signaling from the rod and cone photoreceptors to ON-BCs is lost because the synapse between photoreceptors and ON-BCs is nonfunctional. The consequence is that ON light responses are absent and that the GCs have oscillating burst spike activity. These oscillations most likely originate in AII ACs just as in *rd1* mice [21]. Interaction between fast sodium and potassium channels in AII ACs, in combination with a slow potassium channel, can lead to a bursting spiking behavior with a burst frequency dependent on the AII AC membrane potential [21]. In *rd1* mice, the input to AII ACs is lost with rod and cone degeneration, leading to a change in AII AC membrane potential, which induces oscillations of about 10 Hz. In *nob* mice, AII ACs lose only their ON input. We hypothesize that as a result, the AII AC membrane potential will not shift as far in *nob* mice as in rd1 mice, and the AII ACs oscillations will be slower (5 Hz). The *nob* AII ACs transmit this oscillating signal back to the BC-synaptic terminals and to the GCs, which induces 5-Hz oscillations in both the excitatory and inhibitory inputs of the GCs. Since the sign of the AII AC inputs is opposite in ON-BCs and OFF-BCs, the *nob* ON- and OFF-GCs oscillate in antiphase. In the dark, the AII ACs oscillate independently of each other. A global light stimulus resets all AII ACs and thereby synchronizes the oscillations, leading to synchronized oscillating output to the AOS, where the signal is translated into an oscillating eye movement. AC, amacrine cell; AOS, accessory optic system; BC, bipolar cell; GC, ganglion cell; ON-DSGC, ON direction-selective GC; *rd1*, retinal degeneration 1; SAC, starburst AC; wt, wild type.
(EPS)

S1 Movie. Movie of the eye movements of one of the patients.
(MOV)

Author Contributions

Conceptualization: Beerend H. J. Winkelman, Marcus H. C. Howlett, Maj-Britt Hölzel, Huibert J. Simonsz, Maureen A. McCall, Maarten Kamermans.

Data curation: Beerend H. J. Winkelman, Marcus H. C. Howlett, Maj-Britt Hölzel, Coen Joling, Kathryn H. Fransen, Gobinda Pangeni, Sander Kamermans, Maarten Kamermans.

Formal analysis: Beerend H. J. Winkelman, Marcus H. C. Howlett, Maj-Britt Hölzel, Coen Joling, Kathryn H. Fransen, Gobinda Pangeni, Sander Kamermans, Maureen A. McCall, Maarten Kamermans.

Funding acquisition: Huibert J. Simonsz, Maureen A. McCall, Chris I. De Zeeuw, Maarten Kamermans.

Investigation: Beerend H. J. Winkelman, Marcus H. C. Howlett, Maj-Britt Hölzel, Coen Joling, Kathryn H. Fransen, Gobinda Pangeni, Maureen A. McCall, Maarten Kamermans.

Methodology: Beerend H. J. Winkelman, Marcus H. C. Howlett, Maj-Britt Hölzel, Kathryn H. Fransen, Gobinda Pangeni, Sander Kamermans, Maarten Kamermans.

Project administration: Maarten Kamermans.

Resources: Hiraki Sakuta, Masaharu Noda.

Software: Beerend H. J. Winkelman, Marcus H. C. Howlett.

Supervision: Maureen A. McCall, Chris I. De Zeeuw, Maarten Kamermans.

Writing – original draft: Beerend H. J. Winkelman, Marcus H. C. Howlett, Maj-Britt Hölzel, Maureen A. McCall, Maarten Kamermans.

Writing – review & editing: Beerend H. J. Winkelman, Marcus H. C. Howlett, Maj-Britt Hölzel, Huibert J. Simonsz, Maureen A. McCall, Chris I. De Zeeuw, Maarten Kamermans.

References

1. Brodsky MC, Dell'Osso LF. A unifying neurologic mechanism for infantile nystagmus. JAMA ophthalmology. 2014; 132(6):761–8. https://doi.org/10.1001/jamaophthalmol.2013.5833 PMID: 24525626

2. Optican LM, Zee DS. A hypothetical explanation of congenital nystagmus. Biol Cybern. 1984; 50 (2):119–34. PMID: 6722208

3. Simonsz HJ, Florijn RJ, van Minderhout HM, Bergen AA, Kamermans M. Nightblindness-associated transient tonic downgaze (NATTD) in infant boys with chin-up head posture. Strabismus. 2009; 17 (4):158–64. https://doi.org/10.3109/09273970903396893 PMID: 20001510

4. Ray TA, Heath KM, Hasan N, Noel JM, Samuels IS, Martemyanov KA, et al. GPR179 is required for high sensitivity of the mGluR6 signaling cascade in depolarizing bipolar cells. J Neurosci. 2014; 34 (18):6334–43. https://doi.org/10.1523/JNEUROSCI.4044-13.2014 PMID: 24790204

5. Klooster J, van Genderen MM, Yu M, Florijn RJ, Riemslag FC, Bergen AA, et al. Ultrastructural localization of GPR179 and the impact of mutant forms on retinal function in CSNB1 patients and a mouse model. Invest Ophthalmol Vis Sci. 2013; 54(10):6973–81. https://doi.org/10.1167/iovs.13-12293 PMID: 24084093

6. Morgans CW, Bayley PR, Oesch NW, Ren G, Akileswaran L, Taylor WR. Photoreceptor calcium channels: insight from night blindness. Vis Neurosci. 2005; 22(5):561–8. https://doi.org/10.1017/S0952523805225038 PMID: 16332266

7. Gregg RG, Mukhopadhyay S, Candille SI, Ball SL, Pardue MT, McCall MA, et al. Identification of the gene and the mutation responsible for the mouse nob phenotype. Invest Ophthalmol Vis Sci. 2003; 44 (1):378–84. https://doi.org/10.1167/iovs.02-0501 PMID: 12506099

8. Pardue MT, McCall MA, LaVail MM, Gregg RG, Peachey NS. A naturally occurring mouse model of X-linked congenital stationary night blindness. Invest Ophthalmol Vis Sci. 1998; 39(12):2443–9. PMID: 9804152

9. Gregg RG, Kamermans M, Klooster J, Lukasiewicz PD, Peachey NS, Vessey KA, et al. Nyctalopin expression in retinal bipolar cells restores visual function in a mouse model of complete X-linked congenital stationary night blindness. J Neurophysiol. 2007; 98(5):3023–33. https://doi.org/10.1152/jn.00608.2007 PMID: 17881478

10. Demas J, Sagdullaev BT, Green E, Jaubert-Miazza L, McCall MA, Gregg RG, et al. Failure to maintain eye-specific segregation in nob, a mutant with abnormally patterned retinal activity. Neuron. 2006; 50 (2):247–59. https://doi.org/10.1016/j.neuron.2006.03.033 PMID: 16630836

11. Scalabrino ML, Boye SL, Fransen KM, Noel JM, Dyka FM, Min SH, et al. Intravitreal delivery of a novel AAV vector targets ON bipolar cells and restores visual function in a mouse model of complete congenital stationary night blindness. Human molecular genetics. 2015; 24(21):6229–39. https://doi.org/10.1093/hmg/ddv341 PMID: 26310623

12. Sivyer B, van Wyk M, Vaney DI, Taylor WR. Synaptic inputs and timing underlying the velocity tuning of direction-selective ganglion cells in rabbit retina. J Physiol. 2010; 588(Pt 17):3243–53. https://doi.org/10.1113/jphysiol.2010.192716 PMID: 20624793

13. Vaney DI, Taylor WR. Direction selectivity in the retina. Current opinion in neurobiology. 2002; 12 (4):405–10. PMID: 12139988

14. Borst A, Euler T. Seeing things in motion: models, circuits, and mechanisms. Neuron. 2011; 71(6):974–94. https://doi.org/10.1016/j.neuron.2011.08.031 PMID: 21943597

15. Taylor WR, Vaney DI. New directions in retinal research. Trends in Neurosciences. 2003; 26(7):379–85. https://doi.org/10.1016/S0166-2236(03)00167-X PMID: 12850434

16. Oyster CW, Takahashi E, Collewijn H. Direction-selective retinal ganglion cells and control of optokinetic nystagmus in the rabbit. Vision Res. 1972; 12(2):183–93. https://doi.org/10.1016/0042-6989(72)90110-1 PMID: 5033683

17. Yonehara K, Shintani T, Suzuki R, Sakuta H, Takeuchi Y, Nakamura-Yonehara K, et al. Expression of SPIG1 reveals development of a retinal ganglion cell subtype projecting to the medial terminal nucleus in the mouse. PLoS ONE. 2008; 3(2):e1533. https://doi.org/10.1371/journal.pone.0001533 PMID: 18253481

18. Yonehara K, Ishikane H, Sakuta H, Shintani T, Nakamura-Yonehara K, Kamiji NL, et al. Identification of retinal ganglion cells and their projections involved in central transmission of information about upward and downward image motion. PLoS ONE. 2009; 4(1):e4320. https://doi.org/10.1371/journal.pone.0004320 PMID: 19177171

19. Volgyi B, Deans MR, Paul DL, Bloomfield SA. Convergence and segregation of the multiple rod pathways in mammalian retina. J Neurosci. 2004; 24(49):11182–92. https://doi.org/10.1523/JNEUROSCI.3096-04.2004 PMID: 15590935

20. Choi H, Zhang L, Cembrowski MS, Sabottke CF, Markowitz AL, Butts DA, et al. Intrinsic bursting of AII amacrine cells underlies oscillations in the rd1 mouse retina. J Neurophysiol. 2014; 112(6):1491–504. https://doi.org/10.1152/jn.00437.2014 PMID: 25008417

21. Margolis DJ, Gartland AJ, Singer JH, Detwiler PB. Network oscillations drive correlated spiking of ON and OFF ganglion cells in the rd1 mouse model of retinal degeneration. PLoS ONE. 2014; 9(1):e86253. https://doi.org/10.1371/journal.pone.0086253 PMID: 24489706

22. Aiken SP, Lampe BJ, Murphy PA, Brown BS. Reduction of spike frequency adaptation and blockade of M-current in rat CA1 pyramidal neurones by linopirdine (DuP 996), a neurotransmitter release enhancer. Br J Pharmacol. 1995; 115(7):1163–8. https://doi.org/10.1111/j.1476-5381.1995.tb15019.x PMID: 7582539

23. Schnee ME, Brown BS. Selectivity of linopirdine (DuP 996), a neurotransmitter release enhancer, in blocking voltage-dependent and calcium-activated potassium currents in hippocampal neurons. J Pharmacol Exp Ther. 1998; 286(2):709–17. PMID: 9694925

24. Pattnaik BR, Hughes BA. Effects of KCNQ channel modulators on the M-type potassium current in primate retinal pigment epithelium. Am J Physiol Cell Physiol. 2012; 302(5):C821–33. https://doi.org/10.1152/ajpcell.00269.2011 PMID: 22135213

25. Tsukamoto Y, Omi N. Classification of Mouse Retinal Bipolar Cells: Type-Specific Connectivity with Special Reference to Rod-Driven AII Amacrine Pathways. Front Neuroanat. 2017; 11:92. https://doi.org/10.3389/fnana.2017.00092 PMID: 29114208

26. Yonehara K, Roska B. Motion detection: neuronal circuit meets theory. Cell. 2013; 154(6):1188–9. https://doi.org/10.1016/j.cell.2013.08.027 PMID: 24034242

27. Helmstaedter M, Briggman KL, Turaga SC, Jain V, Seung HS, Denk W. Connectomic reconstruction of the inner plexiform layer in the mouse retina. Nature. 2013; 500(7461):168–74. https://doi.org/10.1038/nature12346 PMID: 23925239

28. Trenholm S, Borowska J, Zhang J, Hoggarth A, Johnson K, Barnes S, et al. Intrinsic oscillatory activity arising within the electrically coupled AII amacrine-ON cone bipolar cell network is driven by voltage-gated Na+ channels. J Physiol. 2012; 590(10):2501–17. https://doi.org/10.1113/jphysiol.2011.225060 PMID: 22393249

29. Marc RE, Anderson JR, Jones BW, Sigulinsky CL, Lauritzen JS. The AII amacrine cell connectome: a dense network hub. Frontiers in neural circuits. 2014; 8:104. https://doi.org/10.3389/fncir.2014.00104 PMID: 25237297

30. Yonehara K, Fiscella M, Drinnenberg A, Esposti F, Trenholm S, Krol J, et al. Congenital Nystagmus Gene FRMD7 Is Necessary for Establishing a Neuronal Circuit Asymmetry for Direction Selectivity. Neuron. 2016; 89(1):177–93. https://doi.org/10.1016/j.neuron.2015.11.032 PMID: 26711119

31. Peachey NS, Ray TA, Florijn R, Rowe LB, Sjoerdsma T, Contreras-Alcantara S, et al. GPR179 is required for depolarizing bipolar cell function and is mutated in autosomal-recessive complete congenital stationary night blindness. Am J Hum Genet. 2012; 90(2):331–9. https://doi.org/10.1016/j.ajhg.2011.12.006 PMID: 22325362

32. Zeitz C, Robson AG, Audo I. Congenital stationary night blindness: an analysis and update of genotype-phenotype correlations and pathogenic mechanisms. Prog Retin Eye Res. 2015; 45:58–110. https://doi.org/10.1016/j.preteyeres.2014.09.001 PMID: 25307992

33. Detwiler PB, Crook JM, Packer O, Robinson F, Dacey DM. The recursive bistratified ganglion cell type of the macaque monkey retina is ON-OFF direction selective [ARVO E-Abstract 3884]. IOVS. 2019; 60.

34. Rodieck RW. Starburst amacrine cells of the primate retina. J Comp Neurol. 1989; 285(1):18–37. https://doi.org/10.1002/cne.902850104 PMID: 2666456

35. Telkes I, Distler C, Hoffmann KP. Retinal ganglion cells projecting to the nucleus of the optic tract and the dorsal terminal nucleus of the accessory optic system in macaque monkeys. Eur J Neurosci. 2000; 12(7):2367–75. https://doi.org/10.1046/j.1460-9568.2000.00133.x PMID: 10947815

36. Stahl JS, James RA, Oommen BS, Hoebeek FE, De Zeeuw CI. Eye movements of the murine P/Q calcium channel mutant tottering, and the impact of aging. Journal of Neurophysiology. 2006; 95(3):1588–607. https://doi.org/10.1152/jn.00318.2005 PMID: 16339008

37. Stahl JS. Calcium channelopathy mutants and their role in ocular motor research. Neurobiology of Eye Movements: From Molecules to Behavior. 2002; 956:64–74.

38. Brainard DH. The Psychophysics Toolbox. Spatial vision. 1997; 10(4):433–6. PMID: 9176952

39. Sagdullaev BT, McCall MA. Stimulus size and intensity alter fundamental receptive-field properties of mouse retinal ganglion cells in vivo. VisNeurosci. 2005; 22(5):649–59.

40. Nobles RD, Zhang C, Muller U, Betz H, McCall MA. Selective glycine receptor alpha2 subunit control of crossover inhibition between the on and off retinal pathways. J Neurosci. 2012; 32(10):3321–32. https://doi.org/10.1523/JNEUROSCI.5341-11.2012 PMID: 22399754

41. Lukasiewicz PD, Eggers ED, Sagdullaev BT, McCall MA. GABA(C) receptor-mediated inhibition in the retina. Vision Res. 2004; 44(28):3289–96. https://doi.org/10.1016/j.visres.2004.07.023 PMID: 15535996

42. Yee CW, Toychiev AH, Sagdullaev BT. Network deficiency exacerbates impairment in a mouse model of retinal degeneration. Frontiers in systems neuroscience. 2012; 6:8. https://doi.org/10.3389/fnsys.2012.00008 PMID: 22383900

43. Quiroga RQ, Nadasdy Z, Ben-Shaul Y. Unsupervised spike detection and sorting with wavelets and superparamagnetic clustering. Neural Comput. 2004; 16(8):1661–87. https://doi.org/10.1162/089976604774201631 PMID: 15228749

44. Simonsz HJ, Gottlob I, Kommerell G, Hergersberg M, Eriksson AW. Frühsymptom bei inkompl. cong. stat. Nachtblindheit und periventrikulärer Leukomalazie. Der Ophthalmologe 1998; 95:178.

45. Pieh C, Simonsz-Toth B, Gottlob I. Nystagmus characteristics in congenital stationary night blindness (CSNB). Br J Ophthalmol. 2008; 92(2):236–40. https://doi.org/10.1136/bjo.2007.126342 PMID: 18227204